

Surface coated red phosphors with silica nanoparticles and silica nanocomposites: performance modifications

Phuc Dang Huu¹, Tri-Vien Vu²

¹Faculty of Fundamental Science, Industrial University of Ho Chi Minh City, Ho Chi Minh City, Vietnam

²Modeling Evolutionary Algorithms Simulation and Artificial Intelligence, Faculty of Electrical and Electronics Engineering, Ton Duc Thang University, Ho Chi Minh City, Vietnam

Article Info

Article history:

Received Jun 15, 2021

Revised Sep 03, 2022

Accepted Sep 13, 2022

Keywords:

Color uniformity

Luminous flux

Mie-scattering theory

SiO₂@LaOF:Eu³⁺

ABSTRACT

Surface coverings using nanomaterials of silica nanoparticles and poly (methyl methacrylate) – abbreviated “PMMA-silica nanomaterials” – are introduced to the Y₂O₂S:Eu³⁺ phosphor through four distinct approaches. The objective is to enhance Y₂O₂S:Eu³⁺ phosphorescence and prolonged sustainability. Using immerse-daubing along with sol-gel approach (Stober way), it is possible to have Y₂O₂S:Eu³⁺ phosphors covered with relatively-monodisperse nano-silica particles (5 nm). To create the silica nano-crystals employed in the coating process of phosphors, we carry out concurrently hydrolysis and condensation procedures to develop the formation and basic polymerization utilizing poly (1-vinyl-2-pyrrolidone). The surface coating layer for Y₂O₂S:Eu³⁺ spheres, which comprises polymethyl methacrylate (PMMA)-silica nanocomposites, can be formed in two ways: by combining silica nanogranules with methyl methacrylate (MMA) monomer as well as through subjecting MMA to tetraethyl orthosilicate (Si(OC₂H₅)₄) chemical compound. The latter approach demonstrated is considered the highest augmentation in phosphorescence and prolonged sustainability for Y₂O₂S:Eu³⁺ spheres. Specifically, when using the second approach to get PMMA-silica phosphor coating, Y₂O₂S:Eu³⁺ exhibited a 5-percent increase in the phosphorescent intensity, compared to untreated phosphors. Contrary to a drop in cathode phosphorescence (CP) output and a rising bombardment duration for exposed phosphor, the latter technique produces a practically constant CP energy with PMMA-silica nanocomposite covered phosphors.

This is an open access article under the [CC BY-SA](https://creativecommons.org/licenses/by-sa/4.0/) license.



Corresponding Author:

Tri-Vien Vu

Modeling Evolutionary Algorithms Simulation and Artificial Intelligence

Faculty of Electrical and Electronics Engineering, Ton Duc Thang University

No. 19 Nguyen Huu Tho Street, Tan Phong Ward, District 7, Ho Chi Minh City, Vietnam

Email: vutrivien@tdtu.edu.vn

1. INTRODUCTION

A wide range of applications of phosphor-integrated light emitting diodes (LED) has been recognized such as the plasma panel, cathode ray tube, and field emission display. The white LEDs utilizing phosphor integration and conversion are especially getting popular as they have several advantages over traditional lighting sources, for example, halogen and incandescent illuminations. These advantages include dependability, saving energy, cheaper maintenance, and enhanced safety [1]–[3]. As for normal white LEDs, a gallium nitride (GaN) blue LED chip packed with a yellow-emitting phosphor material, popular Y₃Al₅O₁₂:Ce (YAG), would be commonly utilized. Unfortunately, due to two-color blending, major disadvantages (for example, hue alteration along with poor color rendering index (CRI) in 60–70 range) seem

to occur with the blue LED and yellow phosphor combination [4]–[6]. LEDs that applied the primary color combination principle of red, blue, and green to perform white lights have become a promising research objective to address these drawbacks. Integrating blue LEDs with red-emitting and green-emitting LEDs or precoating an ultraviolet (UV) LED with green and red phosphors or with three phosphors that have the required basic color emissions can result in white LEDs. Three phosphors, which were employed for precoating near-UV-excitation indium gallium nitride (InGaN)-based LED chip, include the red-emitting $\text{Y}_2\text{O}_2\text{S}:\text{Eu}^{3+}$, blue-emitting $\text{BaMgAl}_{10}\text{O}_{17}\text{Eu}^{2+}$, and green-emitting zinc sulfide (ZnS) [7]–[9]. However, since the red phosphor $\text{Y}_2\text{O}_2\text{S}:\text{Eu}^{3+}$ exhibits weaker photoluminescence (PL) intensity, compared to the PL intensities of the green as well as blue phosphors, it is necessary to have all three phosphors integrated with a high concentration of red phosphors for adequate color rendering. Furthermore, due to its fragility, $\text{Y}_2\text{O}_2\text{S}:\text{Eu}^{3+}$ lifespan is degraded as being excited by a near-UV light source. As a result, for a white LED to improve its coloristic performance, the efficiency-related issues of red phosphors must be resolved. Many researchers performed various tests to resolve the disadvantages of the red-emitting $\text{Y}_2\text{O}_2\text{S}:\text{Eu}^{3+}$. Several rare-earth ion-activated alkaline-earth sulfides (AeS) have been proposed and outperformed the red $\text{Y}_2\text{O}_2\text{S}:\text{Eu}^{3+}$. Nonetheless, the inferior stability of AeS when being exposed to atmospheric factors such as moisture has put a restriction on this material's utilization. Despite the fact that several pieces of research have been conducted to improve AeS robustness and efficiency by modifying their compositions and synthesis processes, the outcomes still need significant improvements. To be suitable for the strict criteria of display devices and LEDs, oxides shells were frequently applied to phosphors. The frequently used oxides include silica, ZnO, Y_2O_3 , MgO, and organic polymers [10]–[13]. Coatings are known as an approach to increasing the bonding strength of phosphors to glass substrates, producing superior phosphors' stability when being under different atmospheric conditions especially moisture, while protecting phosphors from the harm of irradiation.

To limit the drop in PL intensity, the coating must be clear and the individual phosphor particle surfaces must be homogeneously covered with an exact amount of coating. In terms of stability, the uniform layer-like covering would be favored over the non-uniform island-like coating [14]–[16]. Because the former has smaller particles of even size, which is better for producing the phosphor covering layer with non-aggregate-forming monodisperse nanoparticles. Phosphor coating was conducted in this work to create phosphors utilizing four distinct approaches, including immerse-daubing (P1), sol-gel (P2), poly (methyl methacrylate) polymethyl methacrylate (PMMA)-silica coating by combining silica nanogranules with methyl methacrylate (MMA) monomer (P3), along with PMMA-silica coating through subjecting MMA to tetraethyl orthosilicate – P4. These techniques offer significant improvements to the phosphors' performance to outweigh that of the uncoated ones. Here, both P3 and P4 techniques aim at performing the surface covering for the phosphors with PMMA-silica nanocomposites achieved through chemical components' reaction. Particularly, in P3 method, the composition for the coating layer consists of silica (SiO_2) nanoparticles, MMA monomer, and starter [17]–[19]. Meanwhile, the chemical elements needed for P4 method include MMA monomer and tetraethyl orthosilicate (TEOS or $\text{Si}(\text{OC}_2\text{H}_5)_4$). The daubed phosphors' form, photoluminescence (PL) intensity, along with reliability were also examined.

2. PREPARATION AND SIMULATION

2.1. Method of creation

By adjusting the number of reagents, including tetraethyl orthosilicate (TEOS) and water, and the catalyst NH_4OH (ammonium hydroxide), the heat level as well as means used for the chemical reactivity, the magnitude for silica nanogranules became modified. For 1 hour, the reaction was carried out at many different temperature ranges. Previously, we studied in our laboratory the impacts of altering the reactant, solvent, and catalyst levels on the silica diameter. To prevent the formation of aggregates in the reaction of the SiO_2 composite, it is essential to manage to modify the medium along with the temperature for the reaction. It is because the main SiO_2 spheres could perform aggregation when their size is less than around 25 nm. The next part explains the specifics of the reaction processes and their associated outcomes. We utilized a high-resolution transmission electron microscope in order to assess the SiO_2 morphologies and that of $\text{Y}_2\text{O}_2\text{S}:\text{Eu}^{3+}$ phosphor at the pre-coating and post-coating stages (HR-TEM, model: JEM-3010, Japan). 10 transmission electron microscopy (TEM) photos of each sample are acquired from 10 separate specimens for the calculation of the SiO_2 particle sizes [20]–[22]. Subsequently, to support this calculation, the optical inspection application (model: series ver. 4.0, BMI, Korea) was utilized for reading the obtained TEM pictures. An energy dispersive spectroscopy (EDS, model: ED2000, Oxford, England) and a Fourier-transform infrared spectroscopy (model: Magna 750, Nicolet, USA) were employed to validate the silica-coated phosphor (or PMMA-silica nanocomposite). At 30 degrees celsius, the PL measurement for the coated phosphor was performed using one singular-hue photomultiplier monitor (model: LH1751300, ORC, Korea) and an excitation source by a xenon light, which has a specific wavelength of 254 nm and power of 150 [23]. All PL

spectra shown in this work were obtained with bandwidths at the emission slit is 1 nm. For the PL test, five samples of each phosphor were equipped. The findings of all phosphors were averaged after they were examined in duplicate. Modifications for the cathodoluminescence (CL) accompanied by aging duration were recorded when subjected to a bombardment of 10 kilovolts electrical current accompanied by a 45 A/cm² average density for about 30 minutes, to conduct the test of phosphors' long-term stability. Specimens were subjected to aging within one damp incubator with regulated heat level (model: TH-G-180, Jeiotech, Korea) under a temperature of 100 °C along with dampness at 80%. We later assessed adjustments for PL intensity accompanied by aging duration to test heat consistency along with the dampness protection from the phosphors pre as well as post daubing [17]–[19].

2.2. Recreation

The usage of the Lighttools 9.0 program along with Mie-hypothesis [20]–[23] in this work enables the making of white light-emitting diodes (WLEDs) containing two-layer phosphor designs to be easily portrayed through assessing the dispersion for phosphor particles. Besides, this program support investigating the impact of the coated phosphor of SiO₂@Y₂O₂S:Eu³⁺ on the WLED efficiency performed at several correlated temperatures (5600 K – 7000 K). For guaranteeing that the WLED in-cup phosphor setting works properly, SiO₂@Y₂O₂S:Eu³⁺ and YAG:Ce³⁺ phosphors are combined, exhibited by Figure 1. As a result, SiO₂@Y₂O₂S:Eu³⁺, YAG:Ce³⁺, and silicone glues are all included in the WLEDs phosphor layer. In Figure 1(a), the real WLED used for the research is shown. For the simulation details of the WLED, the wiring diagram of the chip cluster is presented in Figure 1(b), the cross-section display for the WLED model will be exhibited by Figure 1(c), and the lighttools-generated 3D model of the WLED is depicted in Figure 1(d).

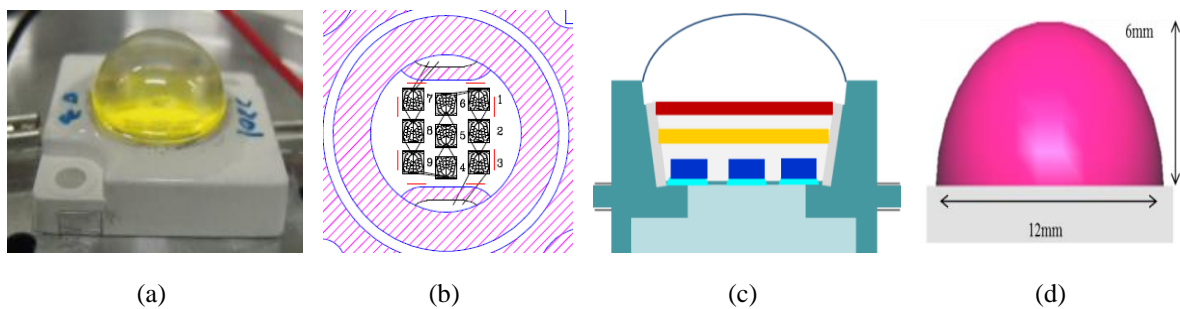


Figure 1. WLED apparatus' illustration: (a) an actual WLED, (b) chip-wiring graph, (c) pc-WLED illustration, and (d) WLED recreation by lighttools software

2.3. Scattering computation

Based on the Mie-dispersion hypothesis, the dispersion coefficient equation $\mu_{sca}(\lambda)$, anisotropy factor $g(\lambda)$, as well as decreased dispersion coefficient $\delta_{sca}(\lambda)$ will be assessed using the (1), (2), and (3) [24], [25].

$$g(\lambda) = 2\pi \int_{-1}^1 p(\theta, \lambda, r) f(r) \cos\theta d \cos\theta dr \quad (1)$$

$$\delta_{sca} = \mu_{sca}(1 - g) \quad (2)$$

Where $N(r)$ will be the diffusional granule distribution density (mm³), C_{sca} indicates the dispersion cross-sections (measured in mm²), $p(\theta, \lambda, r)$ represents the phase function, and the optical wavelength (nm), r represents the dispersing particle radius (μm), θ represents the dispersion angle ($^{\circ}\text{C}$). $f(r)$ represents the diffusive spheres' size distribution function in a phosphor film, and is demonstrated as:

$$f(r) = f_{dif}(r) + f_{phos}(r) \quad (3)$$

The Stober technique was used to create silica nanoparticles with almost monodispersity and spherical shapes. A prior work generated the SiO₂ with a diameter between 10 nm – 450 nm by varying reacting-associated chemical components, including the solvent (ethanol or methanol), reactants' proportion (TEOS and water), as well as catalyst (ammonium hydroxide). We inspected the reduction in the diameter of particles by lowering the concentrations of either NH₄OH or TEOS while adding more water. Using ethanol solvent could produce almost monodispersed SiO₂ nanoparticles with the diameter range of 50 nm – 450 nm, whereas silica

nanoparticles of 10 nm – 50 nm in particle size are probably generated when employing methanol solvent. Owing to changes in the nuclei size in different solvents, particle size is found to vary depending on the specific solvent that is applied. When over 25 nm particles were generated, the silica nanoparticle displaying an almost monodispersed state and spherical shape could be produced. Aggregates are generated with primary silica nanoparticles (network configuration) presenting a particle size that is smaller than 25 nm. In this work, the modification of temperature and medium in the reaction process is introduced to avoid the aggregate formation as well as surging the magnitude degradation for the silica nanogranules.

The influences of reaction heat level on the variations in particle size are subsequently demonstrated as follows. For this investigation, the chemical reaction compound uses the methanol solvent (1 L) for mixing TEOS, NH_4OH , and water, whose concentrations are controlled at 0.28 mol, 10 mol, and 2 mol, respectively. As observed, the temperature increase of the reaction prompts the deduction in the particle size, which eventually becomes stable. Specifically, once the temperature during the reaction is $\geq 80^\circ\text{C}$, the silica nanoparticles are nearly monodispersed and get a size of 10 nm. In other words, the granule magnitude for the silica dwindled (50 nm at 30°C down to 10 nm at approximately 80°C). Particles bigger than 30 nm generated the setting involving almost singularly-diffuse as well as globular nanogranules. In addition, aggregates generated with key silica nanogranules were beneath 20 nm in magnitude. It is possible to clarify such results various in certain ways. When smaller granules get generated, for instance, there are more particles made since diminutive granules possess higher surface tension, surpassing big granules which means these granules quickly combine, forming an exterior with greater stability. Consequently, key silica granules beneath 20 nm in magnitude developed one formation caused by formed aggregates. On the other hand, the silica larger than 20 nm in diameter shows no development of aggregates. Still, difficulties related to aggregate formation cannot be overcome by merely altering the reaction temperature.

Then, the scattering features of the phosphor are analyzed with different particle diameters. The reduced scattering coefficient and scattering cross section of TiO_2 particles are monitored under 450 nm and 550 nm, depicted by Figure 2 and Figure 3, respectively. According to the collected data, the increasing size of the TiO_2 lead to greater reduced scattering coefficient and scattering cross-section, indicating a higher scattering probability which would result in more significant absorption occurrences.

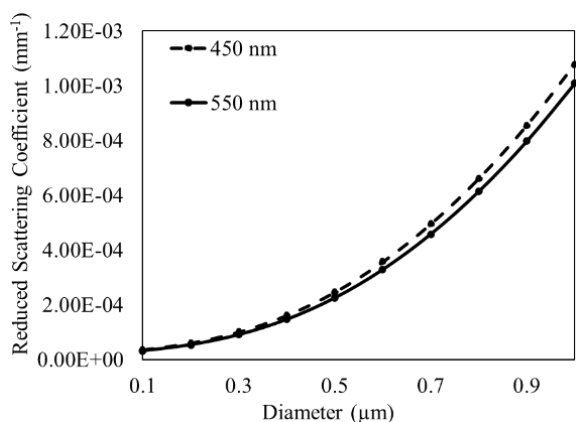


Figure 2. Reduced dispersion coefficient for SiO_2 granules under 450 nm along with 550 nm

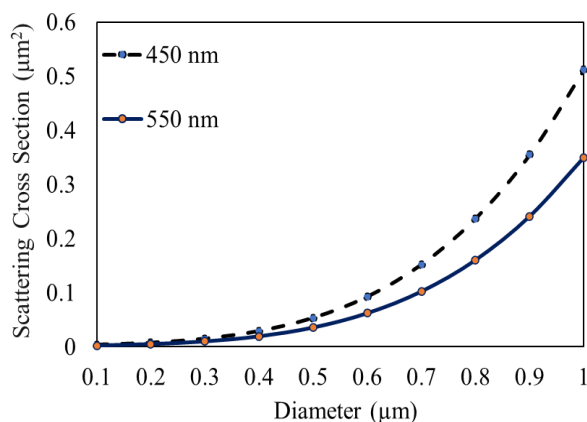


Figure 3. The scattering cross section for SiO_2 granules under 450 nm along with 550 nm

3. RESULTS AND DISCUSSION

To create the silica nanoparticles having less than 20 nm diameter and almost monodisperse state without producing aggregates, the vinylpyrrolidone monomer (VPM) is introduced into the reaction process. In the meantime, the synthesis of silica nano-crystals by hydrolysis and precipitation processes, as well as the creation of polyvinylpyrrolidone (PVP) by radical polymerization, may proceed concurrently with the appropriate quantity of azobisisobutyronitrile (AIBN) initiator. The impact of the temperature during the reaction process on the particle diameter of SiO_2 , as the VPM proportion is constant at 0.2 mol and the AIBN is 0.5 wt% VPM is added, is demonstrated in Figure 4. In spite of the reaction temperatures, the VPM addition leads to the decreasing particle size of silica in the reaction compound. There is no observable aggregate formation with main SiO_2 nanoparticles when their particle diameter is ≥ 10 nm, which is displayed by Figure 5. However, as the particle magnitude for silica is reduced to around 5 nm, aggregates are still produced.

During the reacting process, the concentration of VPM is adjusted between 0.2 nm – 0.4 mol. Meanwhile, the other chemical components are constant in reacting concentrations to avoid aggregate formation. Particularly, the particle size of the silica in nano-composition is further lowered, specifically decreasing from 10 nm to 5 nm, with no aggregate formation noticed. When the particle size is likewise lowered to around 3 nm, no aggregate formation in SiO_2 composite is recorded. It is suggested by these findings that by adding the appropriate quantity of VPM to the reacting composite, aggregation formation is avoidable. Besides, owing to the solubility of PVP in both methanol and water, it is possible to remove the produced SiO_2 nanoparticles easily from the resultant solution by centrifugation. In conclusion, by adding an adequate concentration of VPM, the silica nanoparticle can reach an almost monodisperse state with a particle size < 25 nm and non-primary aggregation. The phosphor coating is then created using 5 nm diameter silica nanoparticles that do not agglomerate.

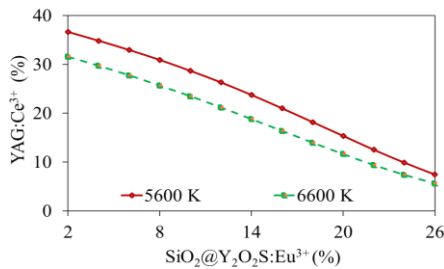


Figure 4. Altering phosphor presence for keeping the average correlated color temperature (CCTs)

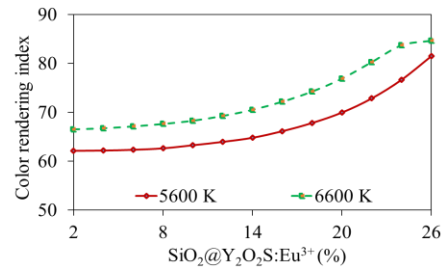


Figure 5. The relation between the color rendering index of WLEDs and concentrations of $\text{SiO}_2@Y_2O_2S:Eu^{3+}$

Luminous performances of the $Y_2O_2S:Eu^{3+}$ phosphor with SiO_2 -nanocomposite shell are examined for changes. The peak intensities of the luminescence obtained from the pre-coated phosphor and post-coated phosphor are around 627 nm, indicating that the emission spectra of phosphors exhibit visible red lights. Regardless of the coating processes, the emission spectrum in the untreated phosphors is relevant to emission spectrum in the coated phosphors [24]. When being surface-coated using either P1 or P2 technique, the PL intensity of the phosphor material somewhat decreases, but will increase when P3 and P4 coating methods are applied. The non-homogeneity of the silica-coated surface of the phosphor when applying the P1 or P2 may easily cause the luminous strength to decline. Organic-inorganic nanocomposite substances are often more transparent than inorganic xerogel. Additionally, because PMMA (1.49) and silica (1.46) have similar refractive indexes, applying PMMA-silica-nanocomposite surface covering can perform higher transparency than using only silica-nanoparticle covering. Reduced optical scattering is caused by a reduction in the disparity of material's refractive indexes at the coating surface. As a result, enhanced transparency may increase emission intensity. Since the lighting-scattering of the SiO_2 nanoparticles in the PMMA matrix can support the diffraction and multiplication of the phosphor-emitted lights, the PL performance can be benefited. Thus, when covered by PMMA-silica nanocomposites, the phosphor probably presents higher luminous output. Besides, the color quality scales (CQS) of the WLED models using the SiO_2 -coated $Y_2O_2:Eu^{2+}$ shown in Figure 6 demonstrates that the SiO_2 coating of $Y_2O_2:Eu^{2+}$ could also improve the color uniformity and rendition of white light as the internal scattering is enhanced. It is possible to attain good CQS of approximately 75 by growing the doped concentration of the phosphor.

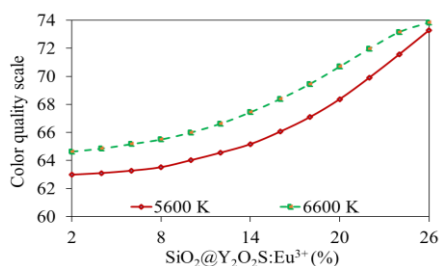


Figure 6. The relation between the color quality scale of WLEDs and concentrations of $\text{SiO}_2@Y_2O_2S:Eu^{3+}$

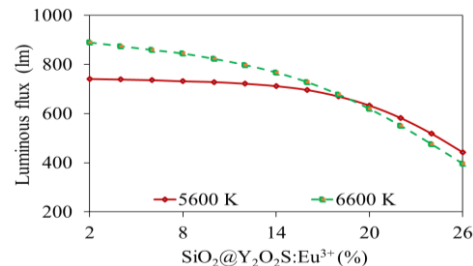


Figure 7. The relation between the luminous flux of WLEDs and concentrations of $\text{SiO}_2@Y_2O_2S:Eu^{3+}$

Cathode phosphorescence (CP) aging research provided the most immediate indication of the phosphor coating's protective properties. For 30 minutes, an electron beam was used to accelerate aging at a 10 kV voltage and a 45 A/cm² current density. Figure 7 depicts the relation between the uncoated/coated phosphors' normalized CL intensity and cumulative aging time. With increasing bombardment duration, the uncoated phosphor's intensity ratio decreased, but it remained almost constant for coated phosphor sphere created by reacting approach P4. The ability to keep the thermal consistency and resistance against moisture of the phosphors is also investigated in two phases: pre-coating and post-coating. Specifically, this investigation is carried out by aging the phosphor spheres in a humidity environment of 80% and at a controlled temperature of 100 °C. The uncoated phosphor's intensity decreased with aging time, but the intensity of coated phosphors (method P4) remained practically constant [25]. These findings suggest that the PMMA-silica nanocomposite covering above the phosphors acted in the form of a shield, slowing surface-related degradation induced by irradiation and air components.

4. CONCLUSION

The surface coating is performed on Y₂O₂S:Eu³⁺ spheres using the composition of nanoparticles SiO₂ or silica through 4 different synthesis techniques. The purpose of getting the phosphor covered with silica is to stimulate its photoluminescent intensity along with high stability for long-term operation. The Stober technique was used to attain the almost monodispersity of 5-nm-diameter SiO₂ nanoparticles in the surface coating film for Y₂O₂S:Eu³⁺ phosphors. The assemblage formation of SiO₂ in the synthesis process is limited by simultaneously executing the hydrolysis and condensation processes and radical polymerization reaction. The hydrolysis and condensation processes are to create silica nano-crystals with TEOS while the reaction of radical polymerization aims at creating PVP from VP monomer. The means of immerse-coating as well as sol-gel perform an uneven SiO₂ daubing above the phosphor spheres' exterior. Meanwhile, the covering presented with the nanocomposite of PMMA and nano-SiO₂ can help achieve the desired uniformity. By reacting TEOS with MMA, a smooth and continuous phosphor shell with PMMA-silica nanocomposite is recognized. The phosphor in the silica shell exhibits a decrease in its PL intensity. Meanwhile, with the PMMA-silica nanocomposite shell, its PL intensity increases. According to the PL comparison between the PMMA-silica-coated and uncoated Y₂O₂S:Eu³⁺ spheres, the coated shows 5% higher than the uncoated ones. In addition, the former had superior stability in long-term utilization over the latter.

REFERENCES

- [1] Y. Zhuang *et al.*, "Effect of phosphor sedimentation on photochromic properties of a warm white light-emitting diode," *Journal of Semiconductors*, vol. 39, no. 12, 2018, doi: 10.1088/1674-4926/39/12/124006.
- [2] C. Sun *et al.*, "Highly efficient Mn-doped CsPb(Cl/Br)₃ quantum dots for white light-emitting diodes," *Nanotechnology*, vol. 31, no. 6, 2020, doi: 10.1088/1361-6528/ab5074.
- [3] X. Yang, M. Zhang, H. Ma, X. Xu, and X. Yu, "Self-crystallized Ba₂LaF₇ laser ceramics with high thermal-stability for white light-emitting-diodes and field emission displays," *ECS Journal of Solid State Science and Technology*, vol. 8, no. 10, 2019, doi: 10.1149/2.0151910jss.
- [4] A. Floriduz and J. D. Devine, "Modelling of proton irradiated GaN-based high-power white light-emitting diodes," *Japanese Journal of Applied Physics*, vol. 57, no. 8, 2018, doi: 10.7567/JJAP.57.080304.
- [5] D. T. Khan *et al.*, "Study on luminescent properties of Tb³⁺ and Sm³⁺ co-doped CaSiO₃ phosphors for white light emitting diodes," *Materials Research Express*, vol. 7, no. 1, 2020, doi: 10.1088/2053-1591/ab5ab8.
- [6] C. Chen *et al.*, "Flexible inorganic CsPbI₃ perovskite nanocrystal-PMMA composite films with enhanced stability in air and water for white light-emitting diodes," *Nanotechnology*, vol. 31, no. 22, 2020, doi: 10.1088/1361-6528/ab7648.
- [7] Y. Zhang, J. Xu, B. Yang, Q. Cui, and T. Tian, "Luminescence properties and energy migration mechanism of Eu³⁺ activated Bi₄Si₃O₁₂ as a potential phosphor for white LEDs," *Materials Research Express*, vol. 5, no. 2, 2018, doi: 10.1088/2053-1591/aaab8a.
- [8] B. G. Kumar *et al.*, "Structural control of InP/ZnS core/shell quantum dots enables high-quality white LEDs," *Nanotechnology*, vol. 29, no. 34, 2018, doi: 10.1088/1361-6528/aac8c9.
- [9] F. Xu *et al.*, "High performance GaN-based hybrid white micro-LEDs integrated with quantum-dots," *Journal of Semiconductors*, vol. 41, no. 3, 2020, doi: 10.1088/1674-4926/41/3/032301.
- [10] A. K. Dubey, V. Kumar, M. Gupta, and D. S. Mehta, "Thermally stable laser-driven phosphor converted white light source using multilayer structured diffuser system," *Laser Physics Letters*, vol. 17, no. 12, 2020, doi: 10.1088/1612-202X/abc759.
- [11] N. T. P. Loan, D. L. Pham, and N. D. Q. Anh, "Enhancement of color quality scale and luminous flux of white LEDs with remote phosphor geometries," *IOP Conference Series: Materials Science and Engineering*, 2019, vol. 617, doi: 10.1088/1757-899X/617/1/012014.
- [12] A. Ali *et al.*, "Blue laser diode-based remote solid-state lighting using plastic optical fiber and phosphor film for a hazardous environment," *ECS Journal of Solid State Science and Technology*, vol. 10, no. 1, 2021, doi: 10.1149/2162-8777/abd51b.
- [13] A. Lenef, M. Raukas, J. Wang, and C. Li, "Phosphor performance under high intensity excitation by InGaN laser diodes," *ECS Journal of Solid State Science and Technology*, vol. 9, no. 1, 2020, doi: 10.1149/2.0352001JSS.
- [14] L. Rosso, S. Tabandeh, G. Beltramino, and V. Fericola, "Validation of phosphor thermometry for industrial surface temperature measurements," *Measurement Science and Technology*, vol. 31, no. 3, 2020, doi: 10.1088/1361-6501/ab4b6b.
- [15] A. K. Dubey, M. Gupta, V. Kumar, V. Singh, and D. S. Mehta, "Blue laser diode-pumped Ce:YAG phosphor-coated cylindrical rod-based extended white light source with uniform illumination," *Laser Physics*, vol. 29, no. 5, 2019, doi: 10.1088/1555-6611/ab05c0.
- [16] F. G. -Santamaria, J. E. Murphy, A. A. Setlur, and S. P. Sista, "Concentration quenching in K₂SiF₆:Mn⁴⁺ phosphors," *ECS Journal*

- of *Solid State Science and Technology*, vol. 7, no. 1, 2018, doi: 10.1149/2.0081801jss.
- [17] Y. H. Kim, N. S. M. Viswanath, S. Unithrattil, H. J. Kim, and W. B. Im, "Review—phosphor plates for high-power LED applications: challenges and opportunities toward perfect lighting," *ECS Journal of Solid State Science and Technology*, vol. 7, no. 1, 2018, doi: 10.1149/2.0181801jss.
- [18] P. S. Dutta, "Full spectrum phosphors for white LEDs and virtual windows for light and health applications," *ECS Journal of Solid State Science and Technology*, vol. 9, no. 1, 2020, doi: 10.1149/2.0422001JSS.
- [19] A. Mendieta, B. Fond, P. Dragomirov, and F. Beyrau, "A delayed gating approach for interference-free ratio-based phosphor thermometry," *Measurement Science and Technology*, vol. 30, no. 7, 2019, doi: 10.1088/1361-6501/ab1b0c.
- [20] S. K. Maurya, R. Kushawaha, S. P. Tiwari, A. Kumar, K. Kumar, and J. C. G. E. da Silva, "Thermal decomposition mediated $\text{Er}^{3+}/\text{Yb}^{3+}$ codoped NaGdF_4 upconversion phosphor for optical thermometry," *Materials Research Express*, vol. 6, no. 8, 2019, doi: 10.1088/2053-1591/ab20b4.
- [21] H. Feuk, D. Sanned, M. Richter, and M. Aldén, "Sources of error for single-shot PMT-based phosphor thermometry in harsh conditions," *Measurement Science and Technology*, vol. 32, no. 8, 2021, doi: 10.1088/1361-6501/abfb1e.
- [22] L. I. D. J. Martin, D. Poelman, P. F. Smet, and J. J. Joos, "Microscopic study of dopant distribution in europium doped SrGa_2S_4 : impact on thermal quenching and phosphor performance," *ECS Journal of Solid State Science and Technology*, vol. 7, no. 1, 2018, doi: 10.1149/2.0341709jss.
- [23] X. Zhu *et al.*, "Synthesis and characterization of Er^{3+} -doped SrNb_2O_6 phosphor for FIR based thermometer," *ECS Journal of Solid State Science and Technology*, vol. 10, no. 4, 2021, doi: 10.1149/2162-8777/abf0ea.
- [24] E. Hertle *et al.*, " $(\text{Gd,Lu})\text{AlO}_3:\text{Dy}^{3+}$ and $(\text{Gd,Lu})_3\text{Al}_5\text{O}_{12}:\text{Dy}^{3+}$ as high-temperature thermographic phosphors," *Measurement Science and Technology*, vol. 30, no. 3, 2019, doi: 10.1088/1361-6501/aafcac.
- [25] A. Kopf, M. Bardi, E. Kohler, T. Endres, G. Bruneaux, and C. Schulz, "Survivability of the thermographic phosphors YAG:Pr and SMP:Sn in a premixed flame," *Measurement Science and Technology*, vol. 32, no. 7, 2021, doi: 10.1088/1361-6501/abf57b.

BIOGRAPHIES OF AUTHORS



Phuc Dang Huu    received a Physics Ph. D degree from the University of Science, Ho Chi Minh City, in 2018. Currently, he is a lecturer at the Faculty of Fundamental Science, Industrial University of Ho Chi Minh City, Ho Chi Minh City, Vietnam. His research interests include simulation LEDs material, renewable energy. He can be contacted at email: danghuophuc@iuh.edu.vn.



Tri-Vien Vu    received a Ph.D. in Mechanical and Automation Engineering from Da-Yeh University, Changhua, Taiwan. Currently, he is working as a lecturer at the Faculty of Electrical and Electronics Engineering, Ton Duc Thang University, Ho Chi Minh City, Vietnam. His research interests are optoelectronics, automation equipment. He can be contacted at email: vutrivien@tdtu.edu.vn.